

Article

Continuous Control Set Model Predictive Control for an Indirect Matrix Converter

Zhengfei Di *, Demin Xu and Kehan Zhang *

School of Marine Science and Technology, Northwestern Polytechnical University, Xi'an 710072, China; xudm@nwpu.edu.cn

* Correspondence: dizhengfei2007@mail.nwpu.edu.cn (Z.D.); zhangkehan210@163.com (K.Z.)

Abstract: A continuous control set model predictive power control strategy for an indirect matrix converter is proposed in this paper. The load reactive power, the load active power, and the input reactive power are controlled simultaneously. This control strategy can obtain output waveforms with fixed switching frequency. Additionally, an optimal switching sequence is proposed to simplify the commutations of the indirect matrix converter. To suppress the input filter resonance, an active damping method is proposed. Experimental results prove that the proposed method features controllable input reactive power, controllable load active and reactive power, fixed switching frequency output waveforms, zero-current switching operations, and effectively suppresses input filter resonance.

Keywords: indirect matrix converter; continuous control set model predictive power control; input filter resonance suppression; optimal switching strategy



Citation: Di, Z.; Xu, D.; Zhang, K. Continuous Control Set Model Predictive Control for an Indirect Matrix Converter. *Energies* **2021**, *14*, 4114. <https://doi.org/10.3390/en14144114>

Academic Editor:
Georgios Konstantinou

Received: 4 May 2021
Accepted: 4 July 2021
Published: 8 July 2021

Publisher's Note: MDPI stays neutral with regard to jurisdictional claims in published maps and institutional affiliations.



Copyright: © 2021 by the authors. Licensee MDPI, Basel, Switzerland. This article is an open access article distributed under the terms and conditions of the Creative Commons Attribution (CC BY) license (<https://creativecommons.org/licenses/by/4.0/>).

1. Introduction

A matrix converter (MC) provides a direct connection between the AC input side and AC output side, in which DC-link capacitors are not employed. It is suitable for many applications with difficult temperatures and pressures due to its simple and compact topology [1,2]. MCs feature many advantages, including controllable input power factor and bidirectional energy flow [3,4]. MCs are usually divided into indirect converters (IMCs) and direct matrix converters (DMCs), which have the same transfer function. In recent years, MCs have been globally discussed and studied in terms of applications, control strategies, topologies, and trends [5–7]. Due to the non-use of DC-link capacitors, MC control complexity has increased; disturbances in the input side affect the output side's power quality. Researchers worldwide have proposed many control schemes for MCs, such as the scalar method, direct torque control, the Venturini method, direct power control, space vector modulation (SVM), and so on [8]. Among them, SVM is a mature control technique for MCs, in which the currents and voltages are represented with input-current vectors and output-voltage vectors, and several fundamental vectors are used for the desired vectors in each sampling instance. The output-voltage vector and the input power factor can be controlled in SVM [9–11].

Currently, with the help of developed power devices and digital processors, finite control set model predictive control (FCS-MPC) is receiving considerable attention, and features many advantages over SVM, such as the ability to consider various constraints and non-linearities, easier implementation and modification based on modern digital processors, and faster dynamic response [12]. In FCS-MPC, a model-based cost function is defined and minimized to determine the switching states and is applied to the power device during the sampling period [13–15]. In [12], a model predictive current control was proposed for a two-level, four-leg inverter without the modulation stage, where the optimal switching states were determined based on the minimization of cost functions. In [13], an FCS-MPC strategy was proposed for four-leg indirect matrix converters and validated

using an experiment, without the use of modulators. In [14], the input reactive power was added into the cost function of the FCS-MPC strategy, and a soft switching sequence was applied for four-leg indirect matrix converters. In [15], a lookup table method using FCS-MPC was proposed for matrix converters, which reduced computational burden.

However, FCS-MPC does not involve a modulation scheme, in which the optimal switching states selected by the cost function may continue to be optimal for the following several sampling instances; thus, the switching frequency is variable, resulting in broad harmonics. To improve this, research considering the combination of FCS-MPC and modulation has been conducted [16–24]. In [16], an indirect model predictive control strategy was proposed for DMCs, in which the imposed sinusoidal current waveforms and the reactive power were considered individually; only simulations were implemented. In [17], a modulated model predictive control (M²PC) strategy was proposed for a DMC, combining the advantages of the space vector modulation and classic predictive control models. Only output currents were controlled and the input side was ignored, an important index for assessment of the control scheme. In [18], a predictive current-error vector control strategy was proposed for DMCs, where both output and input currents were controlled. In [19], an M²PC strategy was proposed for a three-phase active rectifier, where a constant switching frequency was realized based on the modulation of the current vectors, similar as that in conventional SVM. The optimized response was extended to the overmodulation region. In [20], an M²PC strategy with active damping was proposed for IMCs, where the source reactive power and load currents were controlled; only simulation was implemented. In [21], a novel M²PC strategy using voltage-error vector analysis was proposed for a DMC, where the available voltage vectors were reduced in each prediction, leading to reduced calculation efforts. In [22], a time-modulated, model-predictive control strategy was proposed for a neutral point clamped (NPC) converter, which can be operated at a 20 kHz sampling frequency. In [23], a novel M²PC strategy was proposed for a six-phase induction motor, where SVM was used to reduce the steady-state error and improve the (x-y) currents at high operating speeds. In [24], FCS-MPC was proposed for ac-dc matrix converters, where the virtual space vectors were preselected to reduce the calculation efforts, and the effect of parameter mismatch was analyzed.

Input filter resonance has been an important issue for predictive control schemes. Some active damping methods have been introduced and applied [20,25–29]. In [25,26], an active damping method was proposed, which is strictly limited by assuming the independent control of input currents. In [27], another new active damping method was constructed using modified input current references, which cannot directly be used in MPCs, since the damping current involves high-frequency harmonics transferred from the input voltage. In [20,28,29], the input voltage harmonics were added to the output current references, an indirect method with limited efficacy. Additionally, the digital DC-blocker involved affects the system dynamic response and limits parameter adjustment.

This paper proposes a continuous control set model predictive power control (CCS-MPPC) scheme for an indirect matrix converter. Its main contributions are:

1. CCS-MPPC combines controllable load active and reactive power, controllable input reactive power, and fixed switching frequency output waveforms. The comparison between the existing methods and the proposed CCS-MPPC scheme can be seen in Table 1.
2. An optimal switching sequence to simplify the IMC commutation.
3. An active damping method is implemented for the power control system. Table 2 shows a comparison between the proposed active damping technique and existing damping methods.

Table 1. Comparison of existing methods and the proposed continuous control set model predictive power control (CCS-MPPC) scheme.

Method	Switching Frequency	Filters	Control Variables	Validation	Applications
Proposed CCS-MPPC	Fixed	Input and output filters	Input reactive power, load active and reactive power	Experiment	IMC
FCS-MPC in [12–15]	Variable	Input filter	Input and output currents	Experiment	four-leg inverters [12], four-leg MCs [13–15] DMC [16–18,21], active rectifier [19], three-level NPC converter [22,23], AC–DC MCs [24]
M ² PC in [16–19,21–24]	Fixed	Input filter	Input and output currents	Experiment	
M ² PC in [20]	Fixed	Input filter	Source reactive power and output current	Simulation	IMC

Table 2. Comparison of the proposed active damping technique and existing damping methods.

Method	Efficiency	Modified Variables	Control Strategy	Notice
The proposed active damping	High	Input reactive power and load active power	CCS-MPPC	Suitable for model predictive power control
Passive damping in [25,26]	Low	Physical implementation	SVM	Physical implementation
Active damping in [27]	High	Input current	SVM	Not applicable for FCS-MPC
Active damping in [20,28,29]	limited	Output current	M ² PC [20], FCS-MPC [28,29]	Digital DC-blocker involved affects the system dynamic response and limits the parameter adjustment

Table 3 explains the symbols used in this paper.

Table 3. Symbols in this paper.

S_L	The load apparent power
S_i	The input apparent power
q_s	Source reactive power
P_L^*	Unmodified load active power reference
Q_L^*	Unmodified load reactive power reference
Q_i^*	Unmodified input reactive power reference
ΔP_L^*	Active damping component added into P_L^*
ΔQ_i^*	Active damping component added into Q_i^*

2. Indirect Matrix Converter System Model

Figure 1 demonstrates the IMC system power circuit, where the IMC includes the inverter and rectifier stages. An LC filter connects u_s to the input stage, which comprises a capacitor C_{fi} ; an inductor L_{fi} , whose resistance is R_{fi} ; and an output filter L_{fo} , whose resistance is R_{fo} . The passive load of each phase involves R_L and C_L .

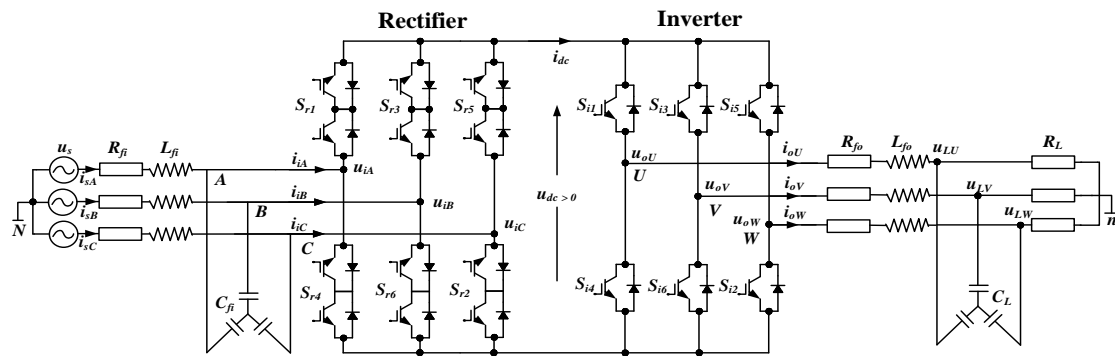


Figure 1. The IMC system power circuit.

From Figure 1, u_{dc} is calculated with S_{ri} and u_i as:

$$u_{dc} = [S_{r1} - S_{r4} \quad S_{r3} - S_{r6} \quad S_{r5} - S_{r2}] u_i \tag{1}$$

$$S_{ri} = \begin{cases} 0, \text{open state} \\ 1, \text{closed state} \end{cases} \tag{2}$$

i_i is calculated with S_{ri} and i_{dc} as:

$$i_i = \begin{bmatrix} S_{r1} - S_{r4} \\ S_{r3} - S_{r6} \\ S_{r5} - S_{r2} \end{bmatrix} i_{dc} \tag{3}$$

Additionally, i_{dc} is calculated with S_{ix} and i_o as:

$$i_{dc} = [S_{i1} - S_{i4} \quad S_{i3} - S_{i6} \quad S_{i5} - S_{i2}] i_o \tag{4}$$

$$S_{ix} = \begin{cases} 0, \text{open state} \\ 1, \text{closed state} \end{cases} \tag{5}$$

The valid switching states are shown in Tables 4 and 5.

Table 4. Rectifier switching states.

V_{dc}	i_A	i_B	i_C	S_{r1}	S_{r2}	S_{r3}	S_{r4}	S_{r5}	S_{r6}
V_{AC}	i_{dc}	0	$-i_{dc}$	1	1	0	0	0	0
V_{BC}	0	i_{dc}	$-i_{dc}$	0	1	1	0	0	0
$-V_{AB}$	$-i_{dc}$	i_{dc}	0	0	0	1	1	0	0
$-V_{AC}$	$-i_{dc}$	0	i_{dc}	0	0	0	1	1	0
$-V_{BC}$	0	$-i_{dc}$	i_{dc}	0	0	0	0	1	1
V_{AB}	i_{dc}	$-i_{dc}$	0	1	0	0	0	0	1

Table 5. Inverter switching states.

i_{dc}	V_{ab}	V_{bc}	V_{ca}	S_{i1}	S_{i2}	S_{i3}	S_{i4}	S_{i5}	S_{i6}
i_a	V_{dc}	0	$-V_{dc}$	1	1	0	0	0	1
$i_a + i_b$	0	V_{dc}	$-V_{dc}$	1	1	1	0	0	0
i_b	$-V_{dc}$	V_{dc}	0	0	1	1	1	0	0
$i_b + i_c$	$-V_{dc}$	0	V_{dc}	0	0	1	1	1	0
i_c	0	$-V_{dc}$	V_{dc}	0	0	0	1	1	1
$i_a + i_c$	V_{dc}	$-V_{dc}$	0	1	0	0	0	1	1
0	0	0	0	1	0	1	0	1	0
0	0	0	0	0	1	0	1	0	1

The model of the input filter is:

$$\begin{cases} \frac{di_s}{dt} = \frac{1}{L_{fi}}(u_s - u_i) - \frac{R_{fi}}{L_{fi}}i_s \\ \frac{du_i}{dt} = \frac{1}{C_{fi}}(i_s - i_i) \end{cases} \quad (6)$$

The passive load of each phase involves R_L and C_L . Thus, the mathematical load model is:

$$\begin{cases} \frac{di_o}{dt} = \frac{1}{L_{fo}}(u_o - u_L) - \frac{R_{fo}}{L_{fo}}i_o \\ \frac{du_L}{dt} = \frac{i_o}{C_L} - \frac{u_L}{C_LR_L} \end{cases} \quad (7)$$

3. Continuous Control Set Model Predictive Power Control Scheme

Figure 2 demonstrates the proposed power control scheme.

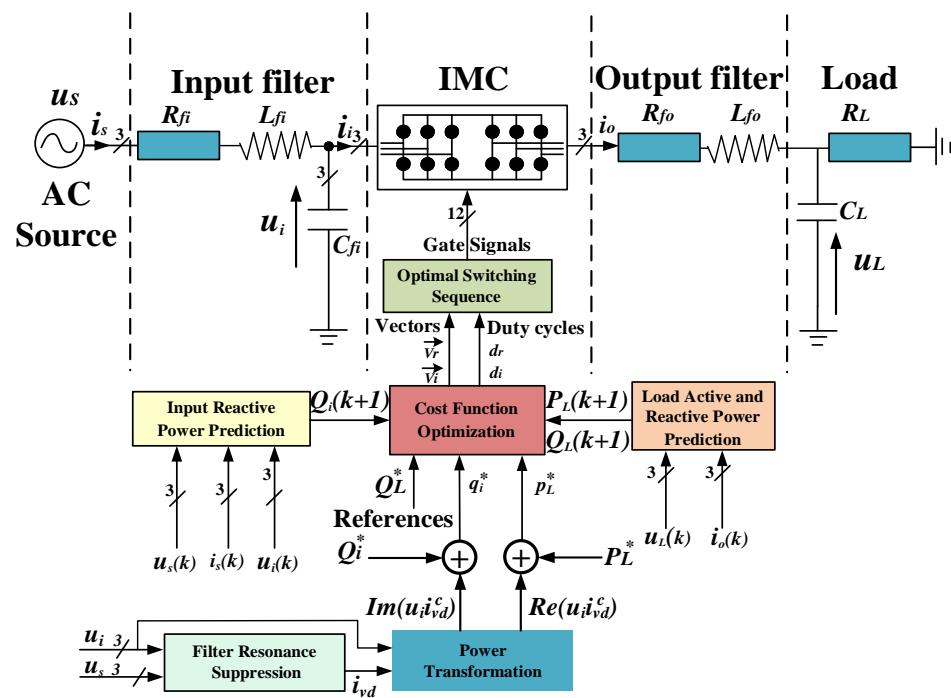


Figure 2. The CCS-MPPC scheme.

Initially, filter resonance suppression updates p_L^* and q_i^* . Then, input reactive, load active, and reactive power predictions generate $Q_i(k + 1)$, $P_L(k + 1)$, and $Q_L(k + 1)$, which are predicted input reactive power, predicted load active power, and predicted load reactive power, respectively. Thus, the input and load cost functions select the optimal vectors V_r , V_i and duty cycles d_r, d_i , which approach their references.

Lastly, the optimal switching sequence is applied similarly to that in SVM. The proposed control strategy is introduced in detail in the following subsections:

3.1. Power Predictions

The load apparent power S_L is:

$$S_L = p_L + jq_L = u_L i_o^c \quad (8)$$

In (8), c represents the complex conjugate.

As shown in Figure 1, source reactive power q_s can be obtained as:

$$\begin{aligned} q_s &= \text{Im}(u_s i_s^c) = \text{Im}\left[\left(u_i + R_{fi} i_s + L_{fi} \frac{di_s}{dt}\right) i_s^c\right] \\ &= \text{Im}\left(u_i i_s^c + L_{fi} \frac{di_s}{dt} i_s^c\right) \\ &= q_i + L_{fi} \frac{di_s}{dt} i_s^c \end{aligned} \quad (16)$$

From Equation (16), it is obvious that q_i and q_s are different because of $L_{fi} \frac{di_s}{dt}$, and usually $L_{fi} \frac{di_s}{dt}$ can be ignored compared to u_s in the LC filter. Hence, q_i and q_s are equal. In addition, q_s usually relies on the prediction of i_s , which is an indirect control. However, from Equation (15), q_i can be directly predicted with the differential equation, which indicates better controllability.

3.2. Cost Function Optimization

The proposed control strategy assesses two cost functions related to two active vectors. Suppose that the cost function of V_{r1} is g_{r1} , and the cost function of V_{r2} (as shown in Figure 3a, V_{r1} and V_{r2} are adjacent vectors) is g_{r2} ; thus

$$\begin{cases} d_{r1} = g_{r2} / (g_{r1} + g_{r2}) \\ d_{r2} = g_{r1} / (g_{r1} + g_{r2}) \\ d_{r1} + d_{r2} = 1 \end{cases} \quad (17)$$

$$g_r = (q_i^* - q_i(k+1))^2 \quad (18)$$

In (17) and (18), g_r represents errors between the input reactive power reference and its predicted value; d_{r1} and d_{r2} are the duty cycles of V_{r1} and V_{r2} , respectively.

With the duty cycles d_{r1} , d_{r2} , the total cost function g_r is:

$$g_r = d_{r1} g_{r1} + d_{r2} g_{r2} \quad (19)$$

In Figure 3b, the implementation of the inverter is similar to that of the rectifier, whereas V_{i0} should be added as well as two nonzero vectors. Suppose the cost function of V_{i0} is g_{i0} , the cost function of V_{i1} is g_{i1} , and the cost function of V_{i2} (V_{i1} and V_{i2} are adjacent vectors) is g_{i2} ; thus,

$$\begin{cases} d_{i0} = g_{i1} g_{i2} / (g_{i0} g_{i1} + g_{i0} g_{i2} + g_{i1} g_{i2}) \\ d_{i1} = g_{i0} g_{i2} / (g_{i0} g_{i1} + g_{i0} g_{i2} + g_{i1} g_{i2}) \\ d_{i2} = g_{i0} g_{i1} / (g_{i0} g_{i1} + g_{i0} g_{i2} + g_{i1} g_{i2}) \\ d_{i0} + d_{i1} + d_{i2} = 1 \end{cases} \quad (20)$$

In (20), d_{i0} , d_{i1} , and d_{i2} are the duty cycles of V_{i0} , V_{i1} , and V_{i2} , respectively; and g_i is:

$$g_i = \lambda_{p_L} (P_L^* - p_L(k+1))^2 + \lambda_{q_L} (Q_L^* - q_L(k+1))^2 \quad (21)$$

In (21), $p_L(k+1)$, $q_L(k+1)$ represent the load active power predicted value and the load reactive power predicted value, respectively; and λ_{p_L} , and λ_{q_L} are weighted factors. With the duty cycles d_{i0} , d_{i1} , and d_{i2} , g_i is calculated as:

$$g_i = d_{i0} g_{i0} + d_{i1} g_{i1} + d_{i2} g_{i2} \quad (22)$$

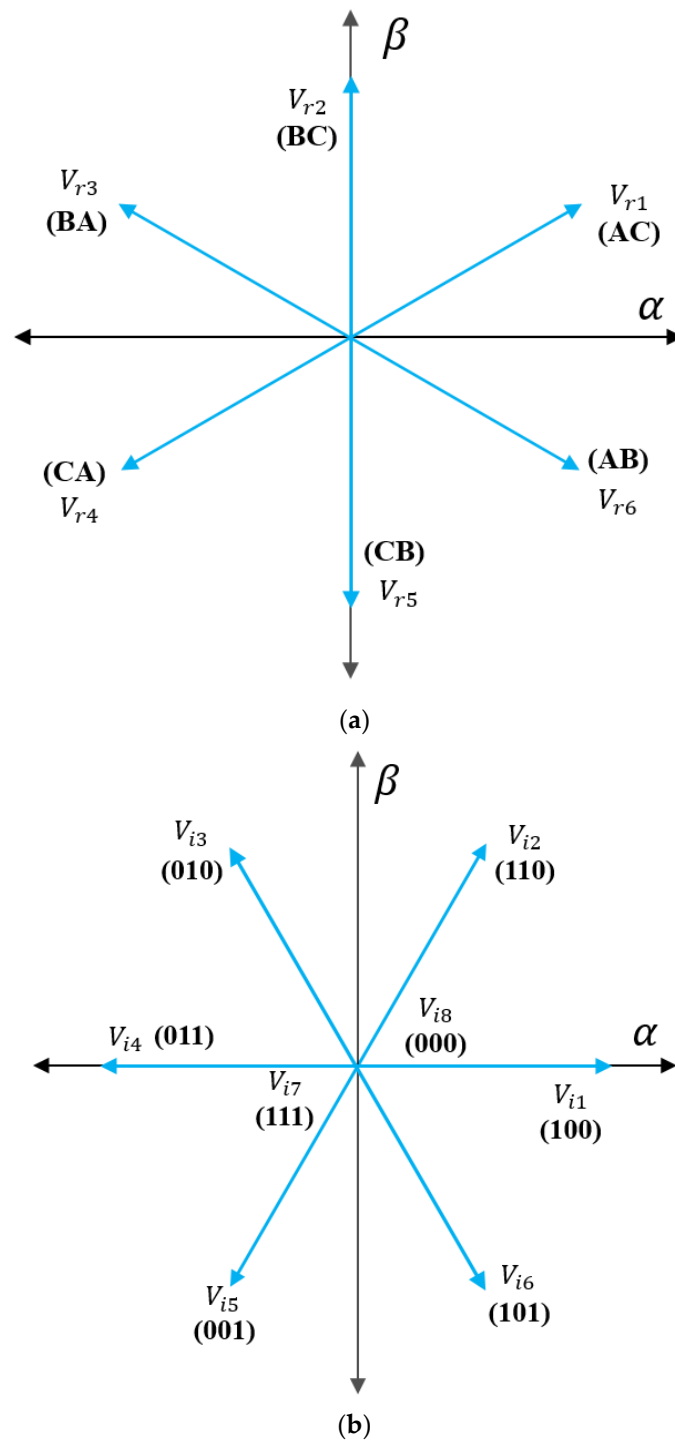


Figure 3. Space vectors for the IMC: (a) for the rectifier; (b) for the inverter.

3.3. Optimal Switching Sequence

This paper proposes an optimal switching sequence to simplify the IMC commutation, as shown in Figure 4.

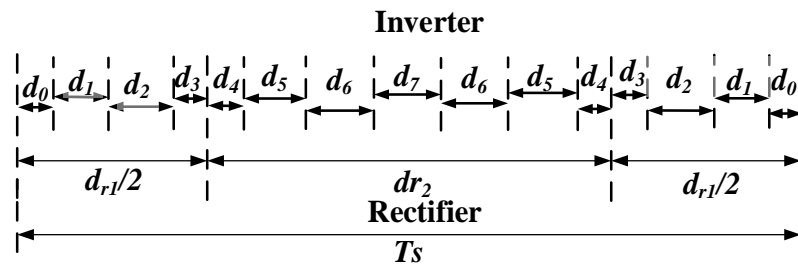


Figure 4. Optimal switching sequence.

$d_0 \sim d_7$ are calculated as:

$$\left\{ \begin{array}{l} d_0 = d_3 = \frac{d_{r1}d_{r2}}{4} \\ d_1 = \frac{d_{r1}d_{r2}}{2} \\ d_2 = \frac{d_{r2}d_{r1}}{2} \\ d_4 = \frac{d_{r1}d_{r2}}{4} \\ d_5 = \frac{d_{r2}d_{r1}}{2} \\ d_6 = \frac{d_{r1}d_{r2}}{2} \\ d_7 = \frac{d_{r1}d_{r2}}{2} \end{array} \right. \quad (23)$$

The duty cycles $d_{r1} \sim d_{r2}$ are calculated as:

$$\left\{ \begin{array}{l} d_{r1} = 2(2d_0 + d_1 + d_2) \\ d_{r2} = 2(d_4 + d_5 + d_6) + d_7 \end{array} \right. \quad (24)$$

From Equations (23) and (24), it is obvious that the rectifier switching states change all the time, when i_{dc} is zero, simplifying the IMC commutation strategy.

4. Input Filter Resonance Suppression

Figure 5 shows three active damping methods. The active damping method I is shown in Figure 5a [25–27], including the virtual resistor R_{vd} . The second method is shown in Figure 5b [20,28,29], where a virtual branch composed of R_{vd} in series with a virtual capacitor C_{vd} is considered in parallel with C_{fi} . Owing to the fundamental frequency components contained in the damping current i_{vd} , the effectiveness of methods I and II is limited. The proposed active damping method is shown in Figure 5c, where a virtual branch with a virtual voltage source of u_s , R_{vd} , and $j\omega_s L_{fi} I_s$ is considered. In $j\omega_s L_{fi} I_s$, ω_s is the source frequency, L_{fi} is the input filter inductance, and I_s denotes the fundamental component in i_s , which is calculated as [30]

$$I_s = (P_L^* + jQ_i^*)u_s / \|u_s\|^2 \quad (25)$$

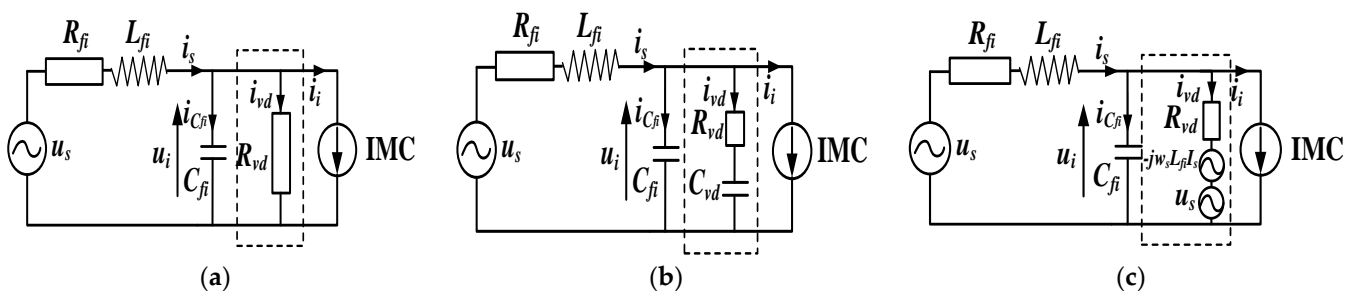


Figure 5. Three active damping methods: (a) method I, (b) method II, and (c) the method in this paper.

From Figure 5c, i_{vd} can be calculated as:

$$i_{vd} = \frac{u_i - u_s + sj\omega_s L_{fi} I_s}{R_{vd}} \quad (26)$$

where the items u_s and $sj\omega_s L_{fi} I_s$ can remove the fundamental component of i_{vd} , and thus the control accuracy will not degrade, and effectiveness will be improved.

The small-signal transfer function can be expressed as:

$$G(s) = \frac{1}{s^2 L_{fi} C_{fi} + s \left(L_{fi} / R_{vd} + \left(1 + R_{fi} / R_{vd} \right) C_{fi} \right) + 1 + R_{fi} / R_{vd}} \quad (27)$$

In Figure 6, the damping coefficient increases when R_{vd} decreases. In addition, the high-frequency magnitude remains the same. Thus, both good filtering and damping performance are realized.

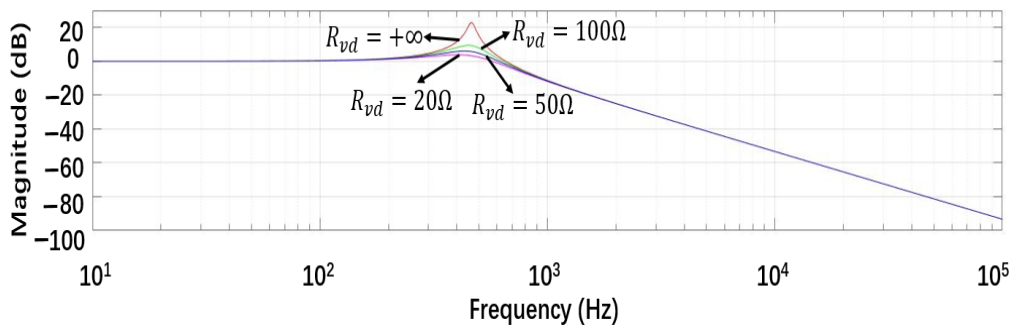


Figure 6. Spectrum of transfer function.

i_s is calculated as:

$$i_s = i_i + i_{C_{fi}} + i_{vd} \quad (28)$$

Thus, the proposed method is implemented by injecting i_{vd} into i_s . In this method, CCS-MPPC controls power directly and the source current indirectly, and s_i is modified as:

$$s_i = u_i i_s^C = u_i \left(i_i^C + i_{C_{fi}}^C \right) + u_i i_{vd}^C \quad (29)$$

Therefore, the real part of $u_i i_{vd}^C$ should be added to the reference of p_i and the imaginary part of $u_i i_{vd}^C$ should be added to the reference of q_i , that is

$$p_i^* = P_i^* + \text{Re}(u_i i_{vd}^C) \quad (30)$$

$$q_i^* = Q_i^* + \text{Im}(u_i i_{vd}^C) \quad (31)$$

Note that the proposed CCS-MPPC strategy scheme controls p_L directly rather than p_i . Thus, (30) should be modified. The reference of p_L can be modified as:

$$q_i^* = Q_i^* + \text{Im}(u_i i_{vd}^C) \quad (32)$$

Finally, the proposed method is implemented by adding the real part of $u_i i_{vd}^C$ to the reference of p_i , and the imaginary part of $u_i i_{vd}^C$ to the reference of q_i .

5. Experimental Results

Figure 7 shows the IMC prototype designed for verification, and Table 6 shows the experiment parameters. The digital controller is composed of an Actel ProASIC3 FPGA and a Texas Instruments C6713 DSP [31].



Figure 7. Laboratory IMC control system prototype.

Table 6. Experimental parameters.

V_s	AC voltage amplitude	141 V
C_{fi}	Input filter capacitor	22 μ F
L_{fi}	Input filter inductor	5 mH
L_{fo}	Output filter inductor	2 mH
C_L	Load capacitor	10 μ F
R_L	Load resistor	20.25 Ω
f_s	Sampling frequency	10 kHz
λ_{pL}	Weighting factor	1
λ_{qL}	Weighting factor	1

Input filter resonances are divided into series (shown in Figure 8a) and parallel resonance (illustrated in Figure 8b) [20,25–29]. The resonant frequency can be calculated with (33) and was designed near the seventh harmonic in this experiment.

$$f_{res} = \frac{1}{2\pi\sqrt{LC}} \approx 7(\text{pu}) \quad (33)$$

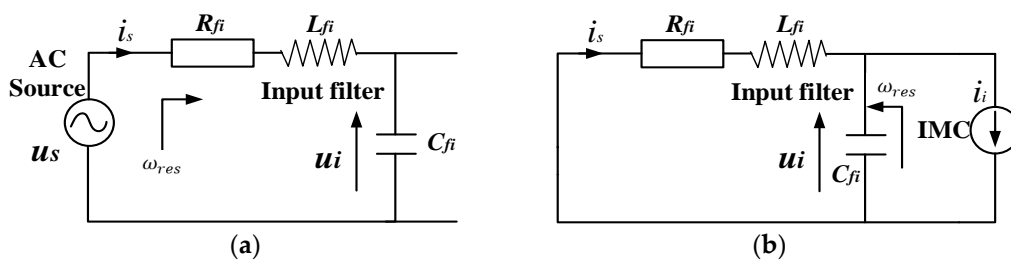


Figure 8. Filter resonances: (a) series resonances and (b) parallel resonances.

Firstly, the FCS-MPC strategy for an IMC without input filter resonance suppression (IFRS) and the optimal switching sequence (OSS) was evaluated, with results shown in Figure 9. In Figure 9, i_{sA} is highly distorted and THD is 38.83%, mainly related to the small damping coefficient. In addition, u_{sA} , u_{LU} , and i_{oU} are affected by the large oscillations of i_{sA} . In Figure 9, resonance needs to be suppressed in terms of power quality for the IMC system.

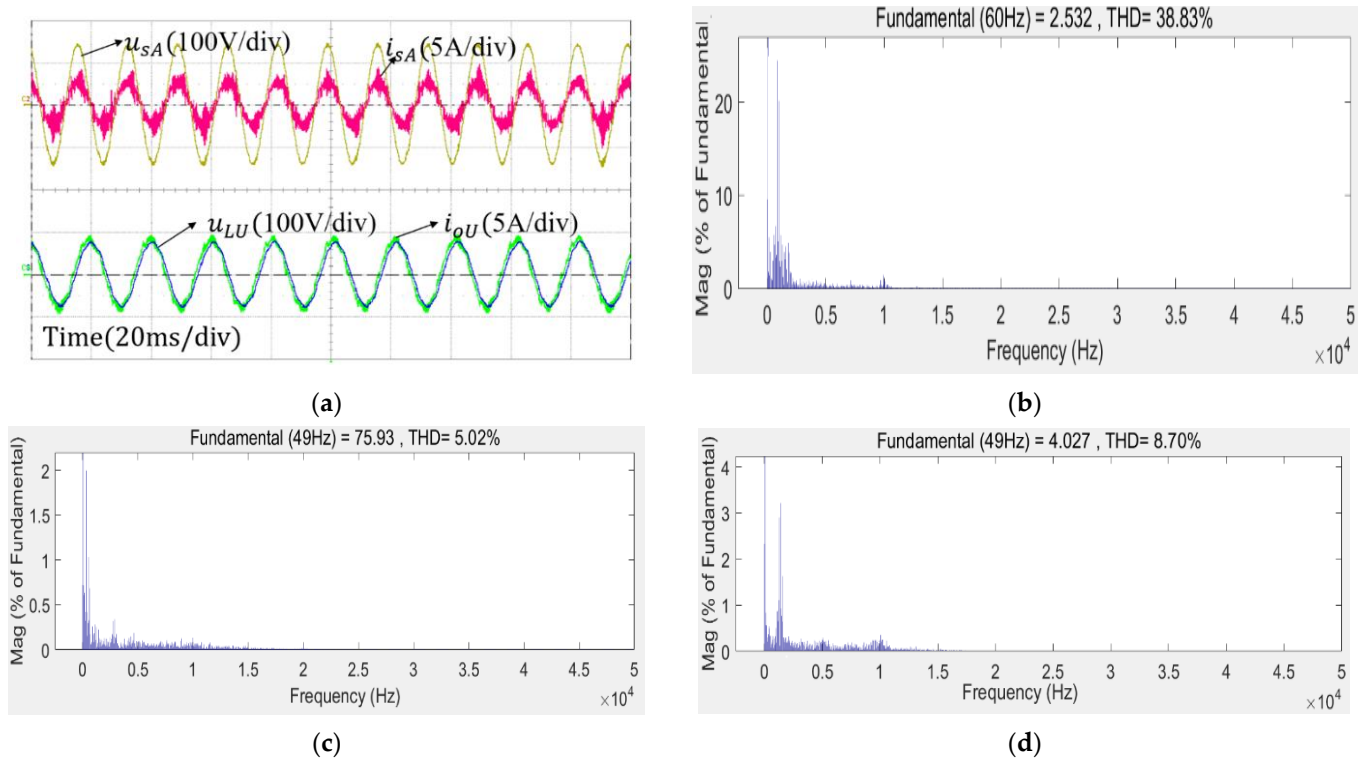


Figure 9. FCS-MPC without IFRS for IMCs: (a) waveforms of u_{sA} , i_{sA} , u_{LU} and i_{oU} ; (b) i_{sA} THD analysis; (c) u_{LU} THD analysis; (d) i_{oU} THD analysis.

Secondly, the experimental results of FCS-MPC with IFRS are demonstrated in Figure 10. The waveform of i_{sA} is significantly improved and its THD is 12.51%; THDs of the load current and voltage are also improved by 7.66% and 4.48%, respectively. In addition, the variable switching frequency phenomenon is shown in Figure 10b–d. In Figure 11, the effects of IFRS with FCS-MPC are demonstrated. In this situation, the input reactive power reference Q_i^* is set to 0 Var, and the load active power reference P_L^* and reactive power reference Q_L^* are set to 450 W and 60 Var, respectively.

Thirdly, experimental results of the CCS-MPPC strategy with IFRS and the OSS are demonstrated in Figures 12 and 13. In this situation, the weighting factors λ_{p_L} and λ_{q_L} in Equation (21) are both set to one, since p_L and q_L are equally important. The waveform of i_{sA} is significantly improved and its THD is 7.45%; the THDs of u_{LU} and i_{oU} are also improved by 6.59% and 3.13%, respectively. The fixed switching frequency phenomenon is observed in Figure 12b–d. At the same time, i_{sA} is in phase with respect to u_{sA} , which indicates q_i is minimized with Equation (18). According to [30], P_L^* and Q_L^* should satisfy the following Equation (34):

$$\begin{cases} P_L^* = 3U_{Lm}^{*2}/2R_L \\ Q_L^* = 3\pi f_o C_L U_{Lm}^{*2} \end{cases} \quad (34)$$

where U_{Lm}^* is the reference of the load voltage amplitude. Thus, based on Equation (34), U_{Lm}^* is obtained at 77.94 V, and f_o is obtained at 50 Hz. In Figure 12, the actual amplitude of the load voltage is 75.41 V, which is 3.26% less than its reference, and the actual output frequency is 49 Hz, which is 2% less than its reference. The reasons for this are as follows:

- (1) According to Equations (8)–(21) and (34), the proposed control algorithm controls u_L and f_o indirectly and controls q_L and p_L directly. The results should be better with the common active load type, where the frequency and amplitude do not need to be controlled.
- (2) The effectiveness of predictive control strategies rely on model accuracy; however, model parameter errors always exist due to the limited capabilities of measuring in-

struments and variations of such parameters with respect to the operating conditions. This effect can be mitigated by improving system parameter robustness [32].

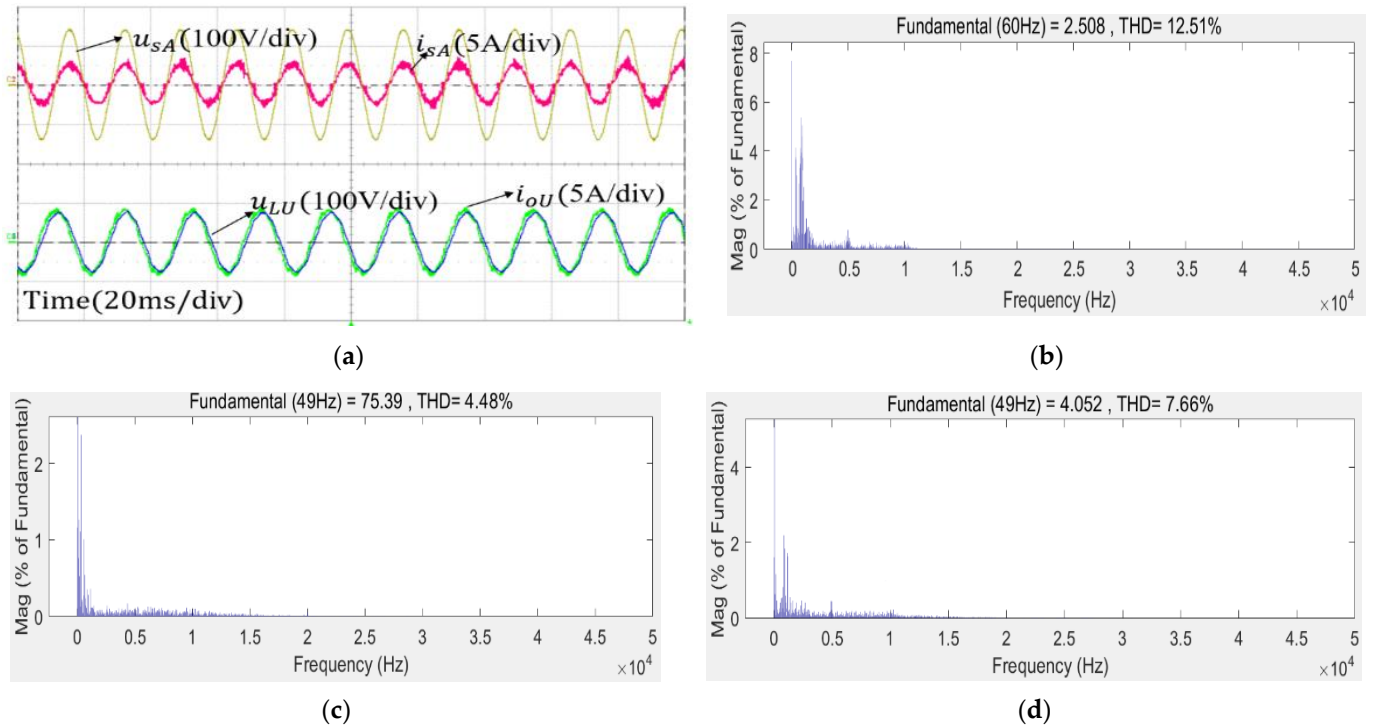


Figure 10. FCS-MPC with IFRS for the IMC: (a) waveforms of u_{sA} , i_{sA} , u_{LU} and i_{oU} ; (b) i_{sA} THD analysis; (c) u_{LU} THD analysis; (d) i_{oU} THD analysis.

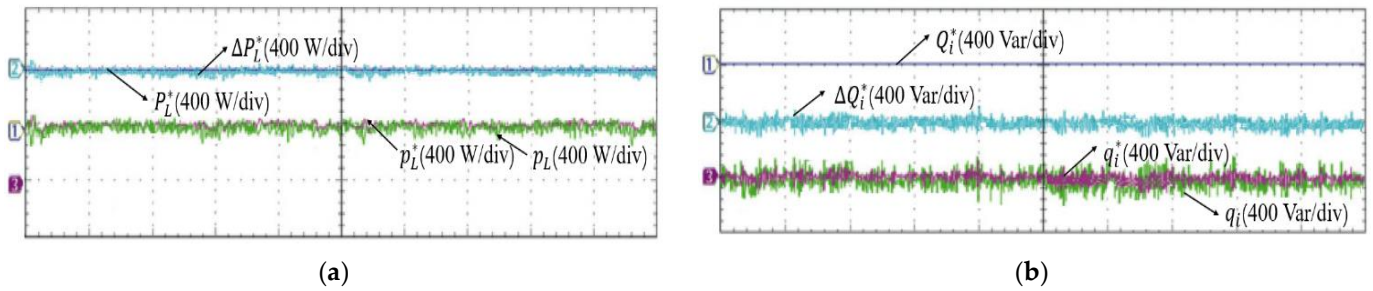


Figure 11. Effects of IFRS with FCS-MPC: (a) the unmodified P_L^* , active damping component ΔP_L^* , the modified p_L^* , and the actual load active power p_L ; (b) the unmodified input reactive power reference Q_i^* , active damping component ΔQ_i^* , q_i , and modified q_i^* .

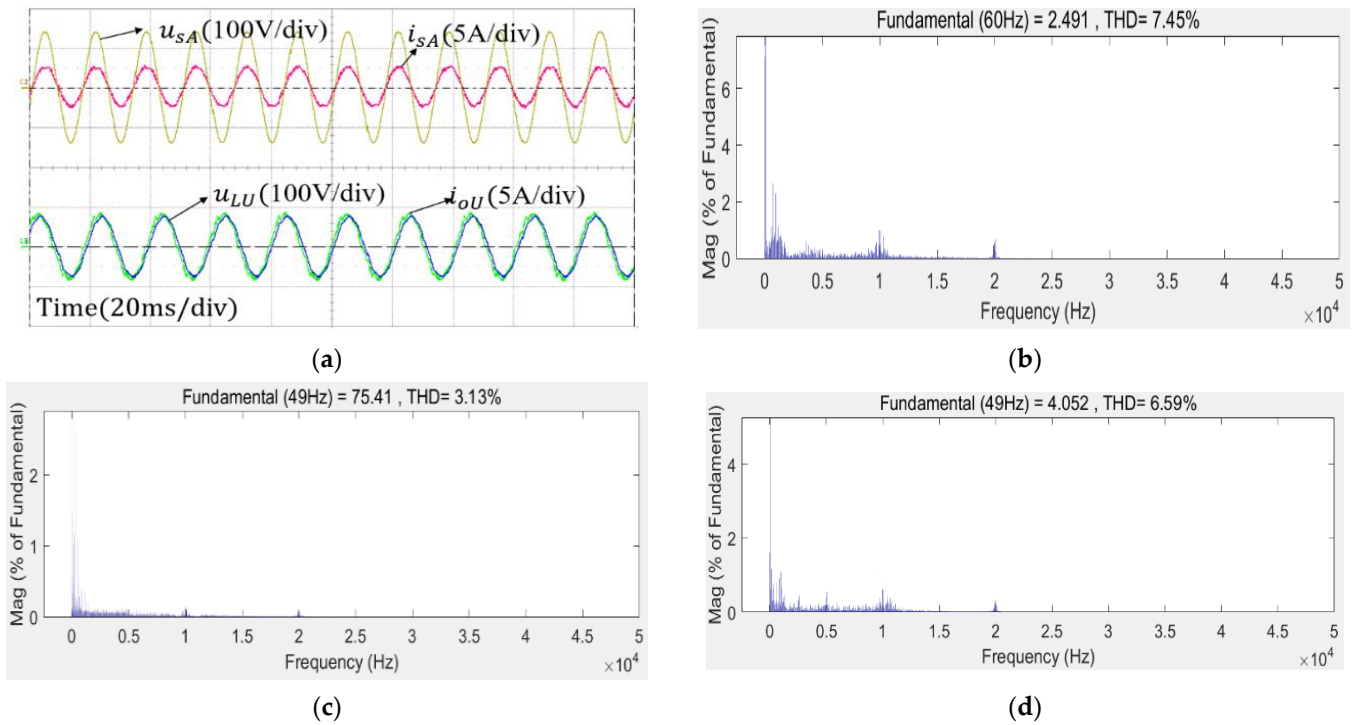


Figure 12. CCS-MPPC with IFRS and OSS for the IMC: (a) waveforms of u_{sA} , i_{sA} , u_{LU} and i_{oU} ; (b) spectrum of i_{sA} ; (c) spectrum of u_{LU} ; (d) spectrum of i_{oU} .

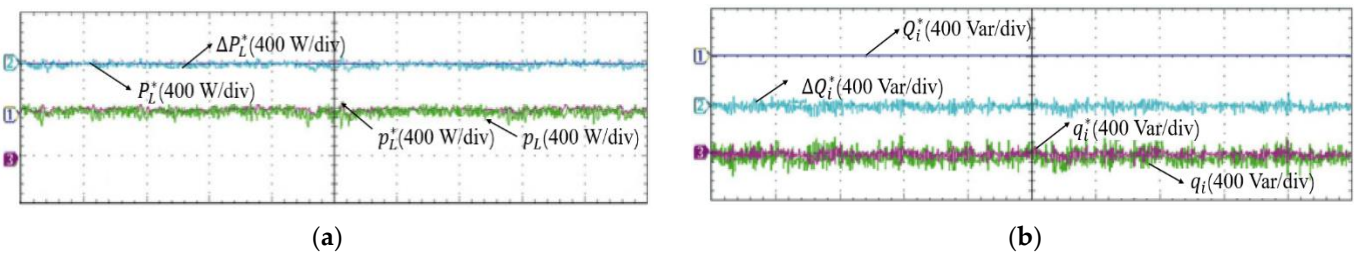


Figure 13. Effects of IFRS with the CCS-MPPC: (a) the unmodified P_L^* , active damping component ΔP_L^* , the modified p_L^* , and actual load active power p_L ; (b) the unmodified Q_i^* , active damping component ΔQ_i^* , input reactive power q_i , and the modified q_i^* .

In addition, define the mean power M_p as:

$$M_p = \frac{1}{m} \sum_{k=1}^m p(k) \tag{35}$$

and define the percentage mean power reference tracking error $\%_{err,p}$ as the absolute difference between actual value of power and its reference:

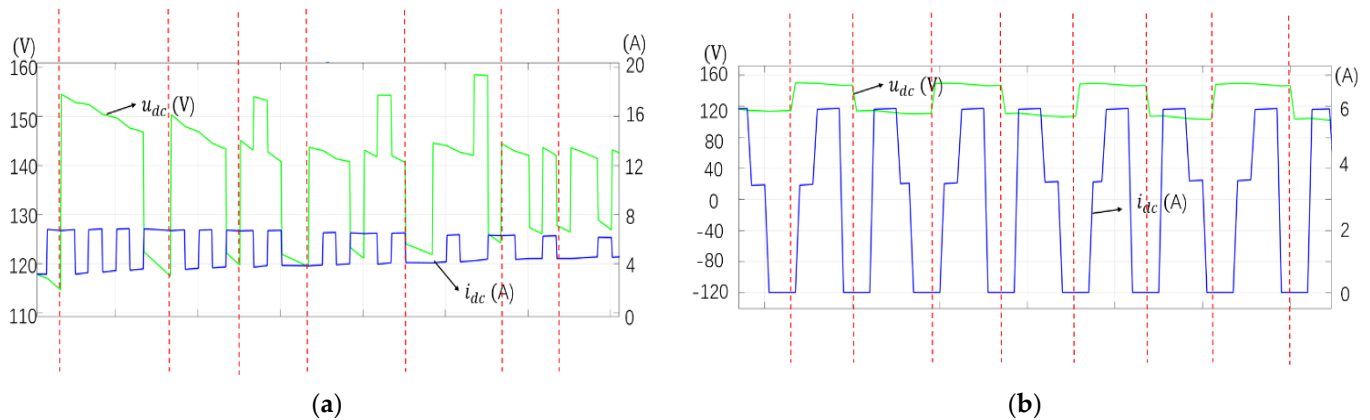
$$\%_{err,p} = \left| \frac{\frac{1}{m} \sum_{k=1}^m p(k)}{P^*} - 1 \right| \tag{36}$$

The comparisons between the FCS-MPC and the proposed CCS-MPPC are shown in Table 7.

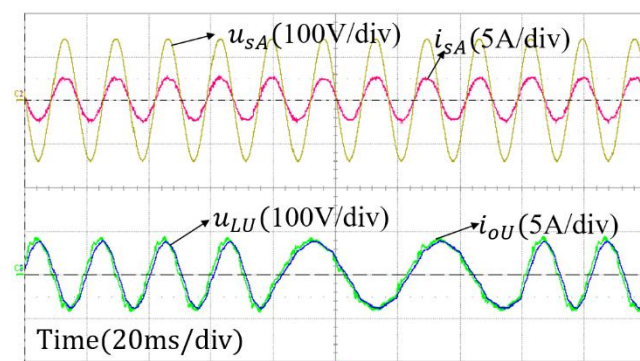
Table 7. Comparisons between FCS-MPC and CCS-MPPC.

	M_{q_i} (Var)	%err, p_L	%err, q_L
FCS-MPC	15.44	5.31%	7.06%
CCS-MPPC	6.63	3.29%	4.52%

Figure 14 demonstrates the waveforms of u_{dc} and i_{dc} with FCS-MPC, and CCS-MPPC with the OSS. As shown in Figure 14a, the rectifier switching state changes when i_{dc} is not zero (red line), and, thus, switching losses are increased. However, with the proposed OSS, the rectifier switching state changes when i_{dc} is zero (red line) in Figure 14b, simplifying the IMC commutation.

**Figure 14.** Waveforms of i_{dc} and u_{dc} : (a) with FCS-MPC; (b) with CCS-MPPC and OSS.

Finally, the transient results of CCS-MPPC with IFRS and OSS are demonstrated in Figures 15–20. Q_L^* is changed between 60 Var and 30 Var in Figure 16, while P_L^* remains unchanged. In Figure 18, P_L^* is changed between 450 W and 225 W, while Q_i^* remains unchanged. In Figure 20, P_L^* is changed between 450 W and 225 W, and Q_i^* is changed between 60 Var and 30 Var at the same time. Accordingly, Figures 15, 17 and 19 show the waveforms of u_{sA} , i_{sA} , u_{LU} , and i_{oU} . As indicated in Figures 15–20, i_{sA} , u_{LU} , and i_{oU} demonstrate almost sinusoidal waveforms, and i_{sA} is in phase with u_{sA} , which indicates q_i is minimized with Equation (18). The dynamic responses are quick.

**Figure 15.** CCS-MPPC with OSS and IFRS for the IMC: waveforms of u_{sA} , i_{sA} , u_{LU} , and i_{oU} .

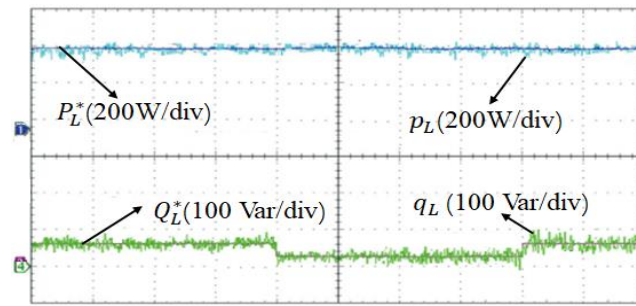


Figure 16. CCS-MPPC with IFRS and OSS for the IMC, where Q_i^* steps between 60 and 30 Var, and P_i^* remains unchanged.

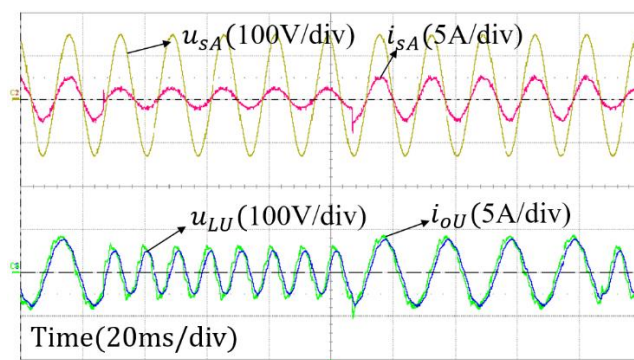


Figure 17. CCS-MPPC with IFRS and OSS for the IMC: waveforms of u_{sA} , i_{sA} , u_{LU} , and i_{oU} .

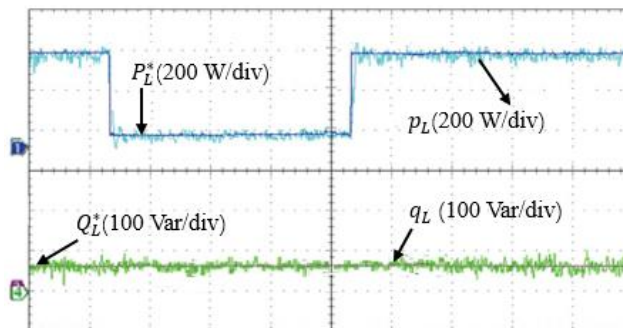


Figure 18. CCS-MPPC with IFRS and OSS for the IMC, where P_L^* steps between 450 and 225 W, and Q_i^* remains unchanged.

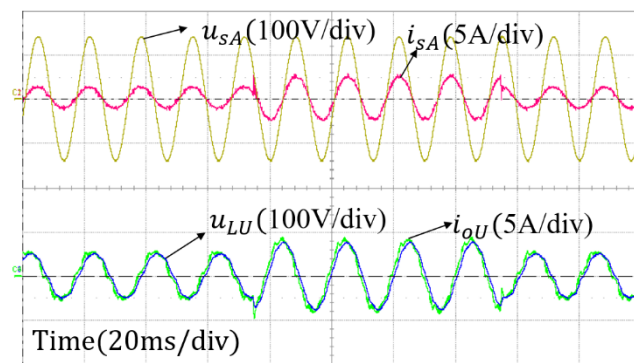


Figure 19. CCS-MPPC with IFRS and OSS for the IMC: Waveforms of u_{sA} , u_{LU} , and i_{oU} .

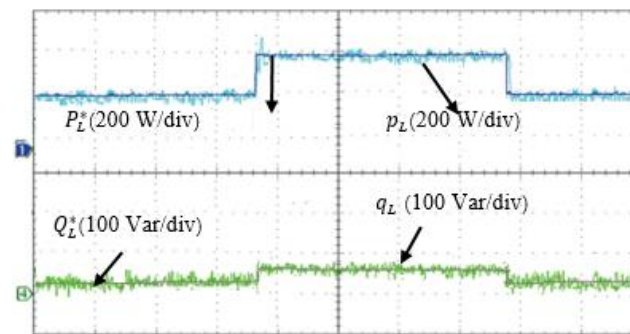


Figure 20. CCS-MPPC with IFRS and OSS for the IMC, where P_L^* steps between 450 and 225 W, and Q_L^* steps between 60 and 30 Var.

6. Conclusions

A continuous control set model predictive power control strategy was proposed. The load reactive power, the load active power, and the input reactive power are controlled at simultaneously. This control strategy can obtain output waveforms with fixed switching frequency.

FCS-MPC does not involve a modulation scheme, in which the optimal switching states may continue to be optimal for the following several sampling instances, and thus the switching frequency is variable, resulting in broad harmonics. To overcome this problem, a suitable vector modulation is added to the model predictive power control by operating at a fixed switching frequency. The CCS-MPPC strategy firstly derives the power prediction model for the IMC. The switching frequency is fixed using two rectifier current vectors and three inverter voltage vectors during a fixed switching interval. The two cost functions in CCS-MPPC differ: the rectifier stage is in relation to input reactive power, and the inverter stage is in relation to load reactive and load active power. Additionally, an optimal switching sequence is proposed to simplify the IMC commutation.

Input filter resonance has been an important issue facing predictive control schemes. To mitigate this problem, an active damping method was proposed; the strategy can be realized by adding the real part of $u_i i_{vd}^C$ to the reference of p_i , and the imaginary part of $u_i i_{vd}^C$ to the reference of q_i .

Experimental results illustrated that the proposed control strategy features controllable input reactive power, controllable load active and reactive power with good tracking to their references, and fixed switching frequency output waveforms. The proposed active damping method effectively suppresses the input filter resonance with better dynamic response and parameter adjustment than the methods in [20,28,29].

Author Contributions: Conceptualization, methodology and validation, Z.D. and D.X.; formal analysis, investigation, resources and writing—original draft preparation, Z.D. and K.Z.; writing—review and editing, supervision and project administration, D.X.; funding acquisition, K.Z. All authors have read and agreed to the published version of the manuscript.

Funding: This work was supported in part by the Natural Science Basic Research Plan in Shaanxi Province of China under Grant 2018JM5033 and in part by the China Scholarship Council under Grant 201606290180.

Acknowledgments: The authors thank the Natural Science Basic Research Plan in Shaanxi Province of China and the China Scholarship Council.

Conflicts of Interest: The authors declare no conflict of interest.

References

1. Alesina, A.; Venturini, M.G.B. Analysis and design of optimum-amplitude nine-switch direct AC-AC converters. *IEEE Trans. Power Electron.* **1989**, *4*, 101–112. [[CrossRef](#)]
2. Wheeler, P.W.; Rodriguez, J.; Clare, J.C.; Empringham, L.; Weinstein, A. Matrix converters: A technology review. *IEEE Trans. Ind. Electron.* **2002**, *49*, 276–288. [[CrossRef](#)]

3. Kolar, J.W.; Friedli, T.; Rodriguez, J.; Wheeler, P.W. Review of Three-Phase PWM AC–AC Converter Topologies. *IEEE Trans. Ind. Electron.* **2011**, *58*, 4988–5006. [[CrossRef](#)]
4. Friedli, T.; Kolar, J.W.; Rodriguez, J.; Wheeler, P.W. Comparative Evaluation of Three-Phase AC–AC Matrix Converter and Voltage DC-Link Back-to-Back Converter Systems. *IEEE Trans. Ind. Electron.* **2012**, *59*, 4487–4510. [[CrossRef](#)]
5. Lee, M.Y.; Wheeler, P.; Klumpner, C. Space-Vector Modulated Multilevel Matrix Converter. *IEEE Trans. Ind. Electron.* **2010**, *57*, 3385–3394. [[CrossRef](#)]
6. Rodriguez, J.; Rivera, M.; Kolar, J.W.; Wheeler, P.W. A Review of Control and Modulation Methods for Matrix Converters. *IEEE Trans. Ind. Electron.* **2012**, *59*, 58–70. [[CrossRef](#)]
7. Lei, J.; Zhou, B.; Bian, J.; Qin, X.; Wei, J. A Simple Method for Sinusoidal Input Currents of Matrix Converter under Unbalanced Input Voltages. *IEEE Trans. Power Electron.* **2016**, *31*, 21–25. [[CrossRef](#)]
8. Rivera, M.; Wheeler, P.; Olloqui, A.; Khaburi, D.A. In A review of predictive control techniques for matrix converters—Part I. In Proceedings of the 2016 7th Power Electronics and Drive Systems Technologies Conference (PEDSTC), Tehran, Iran, 16–18 February 2016; pp. 582–588. [[CrossRef](#)]
9. Sun, Y.; Li, X.; Su, M.; Wang, H.; Dan, H.; Xiong, W. Indirect Matrix Converter-Based Topology and Modulation Schemes for Enhancing Input Reactive Power Capability. *IEEE Trans. Power Electron.* **2015**, *30*, 4669–4681. [[CrossRef](#)]
10. Nguyen, T.D.; Lee, H. A New SVM Method for an Indirect Matrix Converter with Common-Mode Voltage Reduction. *IEEE Trans. Ind. Inform.* **2014**, *10*, 61–72. [[CrossRef](#)]
11. Tsoupos, A.; Khadkikar, V. A Novel SVM Technique with Enhanced Output Voltage Quality for Indirect Matrix Converters. *IEEE Trans. Ind. Electron.* **2019**, *66*, 832–841. [[CrossRef](#)]
12. Rivera, M.; Yaramasu, V.; Llor, A.; Rodriguez, J.; Wu, B.; Fadel, M. Digital Predictive Current Control of a Three-Phase Four-Leg Inverter. *IEEE Trans. Ind. Electron.* **2013**, *60*, 4903–4912. [[CrossRef](#)]
13. Garcia, C.; Rivera, M.; Lopez, M.; Rodriguez, J.; Pena, R.; Wheeler, P.; Espinoza, J. A Simple Current Control Strategy for a Four-Leg Indirect Matrix Converter. *IEEE Trans. Power Electron.* **2015**, *30*, 2275–2287. [[CrossRef](#)]
14. Garcia, C.; Rivera, M.; Rodriguez, J.; Wheeler, P.; Pena, R. Predictive Current Control with Instantaneous Reactive Power Minimization for a Four-Leg Indirect Matrix Converter. *IEEE Trans. Ind. Electron.* **2017**, *64*, 922–929. [[CrossRef](#)]
15. Siami, M.; Khaburi, D.; Rivera, M.; Rodriguez, J. A Computationally Efficient Lookup Table Based FCS-MPC for PMSM Drives Fed by Matrix Converters. *IEEE Trans. Ind. Electron.* **2017**, *65*, 7645–7654. [[CrossRef](#)]
16. Rivera, M.; Toledo, S.; Baier, C.; Tarisciotti, L.; Wheeler, P.; Verne, S. Indirect predictive control techniques for a matrix converter operating at fixed switching frequency. In Proceedings of the 2017 IEEE International Symposium on Predictive Control of Electrical Drives and Power Electronics (PRECEDE), Pilsen, Czech Republic, 4–6 September 2017; pp. 13–18. [[CrossRef](#)]
17. Vijayagopal, M.; Zanchetta, P.; Empringham, L.; Lillo, L.; Tarisciotti, L.; Wheeler, P. Control of a Direct Matrix Converter with Modulated Model-Predictive Control. *IEEE Trans. Ind. Appl.* **2017**, *53*, 2342–2349. [[CrossRef](#)]
18. Vijayagopal, M.; Silva, C.; Empringham, L.; Lillo, L. Direct Predictive Current-Error Vector Control for a Direct Matrix Converter. *IEEE Trans. Power Electron.* **2019**, *34*, 1925–1935. [[CrossRef](#)]
19. Garcia, C.; Silva, C.; Rodriguez, J.; Zanchetta, P.; Odhano, S. Modulated Model-Predictive Control with Optimized Overmodulation. *IEEE J. Emerg. Sel. Top. Power Electron.* **2019**, *7*, 404–413. [[CrossRef](#)]
20. Di, Z.; Rivera, M.; Dan, H.; Tarisciotti, L.; Zhang, K.; Xu, D.; Wheeler, P. Modulated model predictive current control of an indirect matrix converter with active damping. In Proceedings of the 2017 43rd Annual Conference of the IEEE Industrial Electronics Society (IECON), Beijing, China, 29 October–1 November 2017; pp. 1313–1318. [[CrossRef](#)]
21. Xifei, L.; Zhong, Z.; Sai, T.; Chao, Z.; Daming, W.; Jun, W. Modulated Model Predictive Control Based on Voltage-Error Vector Analysis for Direct Matrix Converter. In Proceedings of the 2020 IEEE 9th International Power Electronics and Motion Control Conference (IPEMC2020-ECCE Asia), Nanjing, China, 29 November–2 December 2020; pp. 853–857. [[CrossRef](#)]
22. Qi, W.; Haitao, Y.; Chen, L.; Xiaoyu, L.; Seang, Y.; Tao, Y.; Rivera, M.; Serhiy, B.; Wheeler, P. A Low-Complexity Optimal Switching Time-Modulated Model-Predictive Control for PMSM with Three-Level NPC Converter. *IEEE Trans. Transp. Electrification.* **2020**, *6*, 1188–1198. [[CrossRef](#)]
23. Magno, A.; Jesus, D.; Jorge, R.; Osvaldo, G.; Raul, G.; Rivera, M. A Novel Modulated Model Predictive Control Applied to Six-Phase Induction Motor Drives. *IEEE Trans. Ind. Electron.* **2021**, *68*, 3672–3682. [[CrossRef](#)]
24. Fang, F.; Tian, H.; Li, Y. Finite Control Set Model Predictive Control for AC–DC Matrix Converter with Virtual Space Vectors. *IEEE J. Emerg. Sel. Top. Power Electron.* **2021**, *9*, 616–628. [[CrossRef](#)]
25. Sato, I.; Itoh, J.; Ohguchi, H.; Odaka, A.; Mine, H. An Improvement Method of Matrix Converter Drives under Input Voltage Disturbances. *IEEE Trans. Power Electron.* **2007**, *22*, 132–138. [[CrossRef](#)]
26. Haruna, J.; Itoh, J. Behavior of a matrix converter with a feed back control in an input side. In Proceedings of the 2010 International Power Electronics Conference (ECCE ASIA), Sapporo, Japan, 21–24 June 2010; pp. 1202–1207. [[CrossRef](#)]
27. Lei, J.; Zhou, B.; Qin, X.; Wei, J.; Bian, J. Active damping control strategy of matrix converter via modifying input reference currents. *IEEE Trans. Power Electron.* **2015**, *30*, 5260–5271. [[CrossRef](#)]
28. Rivera, M.; Rodriguez, J.; Wu, B.; Espinoza, J.R.; Rojas, C.A. Current Control for an Indirect Matrix Converter with Filter Resonance Mitigation. *IEEE Trans. Ind. Electron.* **2012**, *59*, 71–79. [[CrossRef](#)]
29. Rivera, M.; Rojas, C.A.; Rodriguez, J.; Wheeler, P.; Wu, B.; Espinoza, J. Predictive Current Control with Input Filter Resonance Mitigation for a Direct Matrix Converter. *IEEE Trans. Power Electron.* **2011**, *26*, 2794–2803. [[CrossRef](#)]

30. Akagi, H.; Watanabe, E.H.; Aredes, M. *Instantaneous Power Theory and Applications to Power Conditioning*; Wiley: Hoboken, NJ, USA, 2007.
31. Trentin, A.; Empringham, L.; Lillo, L.; Zanchetta, P.; Wheeler, P.; Clare, J. Experimental Efficiency Comparison Between a Direct Matrix Converter and an Indirect Matrix Converter Using Both Si IGBTs and SiC mosfets. *IEEE Trans. Ind. Appl.* **2016**, *52*, 4135–4145. [[CrossRef](#)]
32. Zhang, X.; Zhang, L.; Zhang, Y. Model Predictive Current Control for PMSM Drives with Parameter Robustness Improvement. *IEEE Trans. Power Electron.* **2019**, *34*, 1645–1657. [[CrossRef](#)]